Neuron, Vol. 42, 757–771, June 10, 2004, Copyright ©2004 by Cell Press

Modulation of Glutamate Mobility Reveals the Mechanism Underlying Slow-Rising AMPAR EPSCs and the Diffusion Coefficient in the Synaptic Cleft

Thomas A. Nielsen, David A. DiGregorio, and R. Angus Silver*
Department of Physiology
University College London
Gower Street
London WC1E 6BT
United Kingdom

Summary

Fast- and slow-rising AMPA receptor-mediated EPSCs occur at central synapses. Fast-rising EPSCs are thought to be mediated by rapid local release of glutamate. However, two controversial mechanisms have been proposed to underlie slow-rising EPSCs: prolonged local release of transmitter via a fusion pore, and spillover of transmitter released rapidly from distant sites. We have investigated the mechanism underlying slow-rising EPSCs and the diffusion coefficient of glutamate in the synaptic cleft (D_{glut}) at cerebellar mossy fiber-granule cell synapses using a combination of diffusion modeling and patch-clamp recording. Simulations show that modulating D_{glut} has different effects on the peak amplitudes and time courses of EPSCs mediated by these two mechanisms. Slowing diffusion with the macromolecule dextran slowed slow-rising EPSCs and had little effect on their amplitude, indicating that glutamate spillover underlies these currents. Our results also suggest that under control conditions D_{glut} is approximately 3-fold lower than in free solution.

Introduction

The time course of synaptic conductances is important for information processing in the brain, because it determines such basic properties as temporal precision and reliability (Cathala et al., 2003; Galarreta and Hestrin, 2001; Harsch and Robinson, 2000) and the gain of rate-coded signals (Mitchell and Silver, 2003). Classical investigations of the neuromuscular junction have led to a model of synaptic transmission where rapid fusion of vesicles with the presynaptic membrane releases neurotransmitter into the synaptic cleft, thereby locally activating postsynaptic receptors and producing fast-rising synaptic conductance changes (Hartzell et al., 1975; Heuser et al., 1979; Katz, 1969; Torri-Tarelli et al., 1985). Recent studies have estimated that 90% of vesicular content enters the synaptic cleft in less than 100 μs (Stiles et al., 1996). At central glutamatergic synapses, the rapid rise time of AMPA receptor (AMPAR)-mediated synaptic currents (Finkel and Redman, 1983; Forti et al., 1997; Geiger et al., 1997; Silver et al., 1992) and time course of displacement of competitive antagonists (Clements, 1996; Diamond and Jahr, 1997) suggest that glutamate release can occur on a similar timescale. However, AMPAR-mediated conductances with slow rise times recorded both from synapses at room temperature (Choi et al., 2000; Renger et al., 2001) and near physiological temperature (Carter and Regehr, 2000; DiGregorio et al., 2002; Schoppa and Westbrook, 2001) indicate the presence of prolonged low concentrations of glutamate in the synaptic cleft.

At least two mechanisms could produce prolonged low concentrations of neurotransmitter: prolonged local release (PLR) via a narrow fusion pore, also known as "slow kiss-and-run," and diffusion of neurotransmitter from distant sites ("spillover"). However, previous studies have not been able to experimentally differentiate between these two mechanisms (Choi et al., 2000; DiGregorio et al., 2002; Renger et al., 2001). Moreover, modeling studies have predicted a wide range of activation of synaptic AMPARs following glutamate release at a neighboring release site (Barbour, 2001; Franks et al., 2002; Rusakov, 2001). Results from these studies suggest that D_{glut} is crucial for understanding the actions of glutamate, because it determines the proportion of receptors activated both within the active zone and at neighboring synapses. A wide range of values for this fundamental synaptic parameter has been proposed (ranging from 0.2 to 1.0 $\mu m^2/ms$ at physiological temperature; Barbour, 2001; Choi et al., 2003; Franks et al., 2002; Rusakov, 2001), but D_{glut} has not yet been experimentally determined. It is therefore unclear from theoretical studies whether the relatively large slow-rising AMPAR EPSCs could be mediated by spillover even when vesicles are released from multiple distant synapses. Evidence for PLR is also controversial. Direct measurements of vesicle fusion in neuroscretory cells using capacitance have demonstrated that in small clear vesicles narrow pores form in a low proportion of fusion events (Klyachko and Jackson, 2002). At central excitatory synapses, results from conflicting optical measurements of single vesicle fusion suggest that kiss-and-run modes may comprise either a minor (Zenisek et al., 2002) or major proportion of release events (Aravanis et al., 2003; Gandhi and Stevens, 2003). Unfortunately, the time course of neurotransmitter release from these fusion events is not known. Thus, it has not been possible to unambiguously distinguish rapid release from distant sites, filtered by diffusion, from PLR (see Jahr, 2003).

The mean AMPAR-mediated EPSC at the cerebellar mossy fiber-granule cell (MF-GC) synapse is mediated by two distinct components, a fast-rising current and a slow-rising current, which are both mediated by receptors located in the postsynaptic density (PSD; DiGregorio et al., 2002). The low variability and large charge transfer of slow-rising EPSCs suggest that they contribute to the reliability of transmission. Here we demonstrate with simulations that lowering D_{glut} can be used to distinguish between PLR and transmitter spillover as the mechanism underlying slow-rising currents. By reducing D_{glut} with the macromolecule dextran and recording EPSCs, we show that spillover is responsible for slow-rising currents at the MF-GC synapse and that

*Correspondence: a.silver@ucl.ac.uk

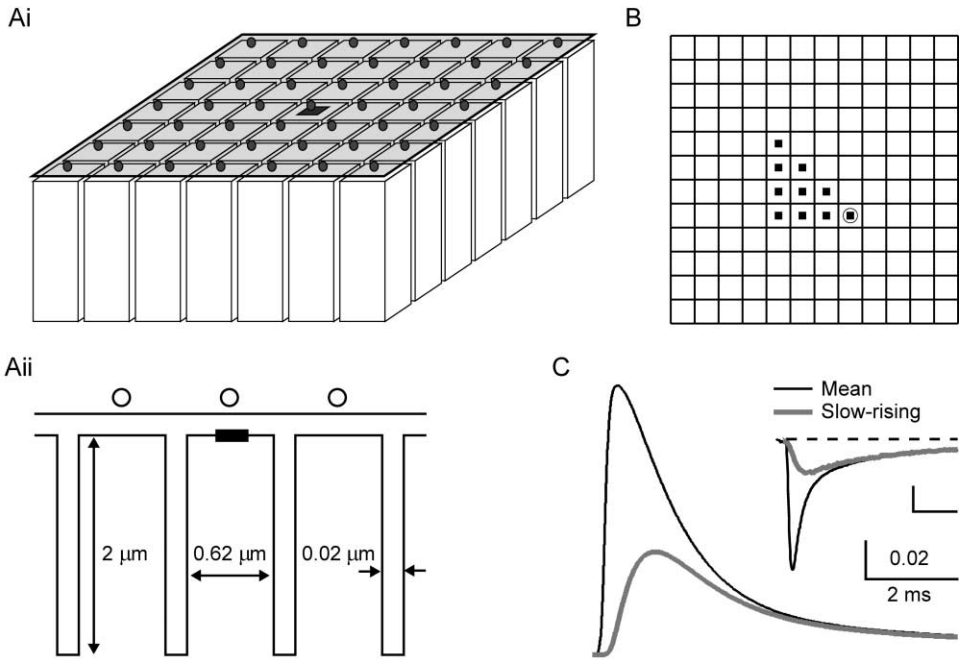

Figure 1. Simulation of Glutamate Diffusion and Receptor Activation for Rapid Local and Distant Release at the MF-GC Synapse

(Ai) Schematic representation of part of the 3D geometry used for simulation of glutamate diffusion. Spheres denote presynaptic release sites, gray shading indicates presynaptic membrane, and columns represent dendritic claws. Glutamate was detected over the central postsynaptic density (dark gray square).

(Aii) Cross-section of the 3D geometry illustrating the sinks created by the space between dendritic claws.

(B) Top view of the actual diffusional space (12 × 12 claws), showing the location of the glutamate source (circle) and multiple detection sites (filled squares) used to calculate concentration transients from each site. We calculated the $[glut]_{cleft}$ waveform arising from multiple sites by summating the individual waveforms detected from each of the ten different release site to central PSD distances (squares) in our diffusional geometry.

(C) Simulated mean and slow-rising responses expressed as AMPAR open probability for the geometry in (A). Responses were calculated with the WJ AMPAR kinetic scheme and a D_{glut} = 0.5 μm^2/ms. Inset: population mean EPSC and slow-rising current recorded from granule cells at 37°C from DiGregorio et al. (2002). Scale bar, 10 pA and 2 ms.

D_{glut} in the synaptic cleft is substantially lower than in free solution.

Results

We first examined whether PLR and spillover of glutamate are physically plausible as mechanisms for slow-rising AMPAR-mediated currents using simulations of glutamate release, diffusion, and receptor activation at the MF-GC synapse.

Geometry of the Diffusional Space at the MF-GC Synapse

Cerebellar MF terminals are large, with hundreds of active zones (Jakab, 1989; Jakab and Hamori, 1988; Xu-Friedman and Regehr, 2003) contacting approximately 50 different GCs. The three to five claw-like structures at the end of a GC dendrite each receive one synaptic contact. To develop a realistic model of glutamate diffusion within the MF-GC cleft, we constructed a simplified three-dimensional diffusional space that captured the essential anatomical features of this synaptic connection, including the diffusional sink of the extracellular space between claws. Figure 1Ai shows a schematic representation of part of the diffusional space, where long rectangular columns represent dendritic claws, the gray surface represents the MF terminal membrane, and the spheres indicate locations of release sites. The dimensions are illustrated in Figure 1Aii, which shows a cross-section of part of the model geometry. We modeled a regular array of 49 release sites with a synaptic cleft width of 20 nm and an intersite distance of 0.64 μm, calculated from a release site density of 2.5 sites/μm^2 as measured from a 3D serial reconstruction of the MF-GC synapse (Xu-Friedman and Regehr, 2003).

We assumed linear diffusion in the synaptic cleft, since block of glutamate transporters does not affect the mean EPSC waveform at early times or the amplitude of slow-rising currents relative to the mean EPSC at the MF-GC synapse (DiGregorio et al., 2002). Moreover, glutamate transporters are located on glial cells (Chaudhry et al., 1995), which are distant from MF release sites (DiGregorio et al., 2002; Xu-Friedman and Regehr, 2003), and buffering by the glutamate binding sites on AMPARs is thought to make negligible contributions to postsynaptic currents (Barbour, 2001). Rapid local release (RLR) of a vesicle at an individual release site was simulated by releasing 4000 glutamate molecules (Riveros et al., 1986) instantaneously into a single voxel.

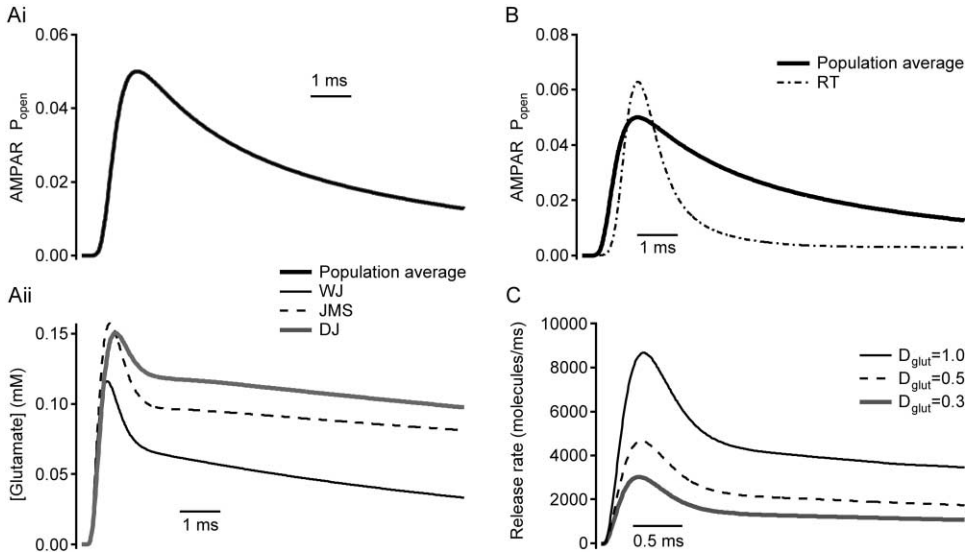

Figure 2. Estimation of Cleft Glutamate Concentration and Prolonged Local Release Time Course from Slow-Rising EPSCs

(Ai) Measured slow-rising current, expressed as AMPAR open probability [$P_{open}(t)$] together with optimized $P_{open}(t)$ waveforms for the WJ, JMS, and DJ kinetic schemes. All waveforms overlie.

(Aii) Concentration waveforms underlying optimal $P_{open}(t)$ waveforms in (Ai).

(B) Measured slow-rising $P_{open}(t)$ and optimized $P_{open}(t)$ waveforms for the RT scheme.

(C) Local glutamate release time course calculated by deconvolving the concentration waveform derived using the WJ scheme with the impulse response function for local release calculated from the 3D geometry in Figure 1A for different values for D_{glut} (units of μm^2/ms).

Simulations of EPSCs Arising from Distant Release Sites

To examine whether measured slow-rising currents could arise from glutamate spillover, we modeled rapid release from many spatially distributed release sites (Figure 1Ai, spheres) and detected glutamate at a single PSD (Figure 1Ai, square). It was possible to simplify the computation of the glutamate concentrations, since several sites had the same distance to the PSD (Figure 1B). This was achieved by calculating the contribution to $[glut]_{cleft}$ from release at each site by sampling a single release event at multiple different synaptic locations (Figure 1B). For these initial simulations, we used a value of D_{glut} of 0.5 μm^2/ms (half the diffusion coefficient of glutamine in aqueous solution at 37°C; calculated from Longsworth, 1953). To simulate vesicular release following an action potential, each release site was modeled stochastically using the measured release probability and latency distribution for vesicular release (Experimental Procedures). For each trial, the $[glut]_{cleft}$ waveform was calculated by summing the glutamate concentrations arising from all sites that released. Since the kinetic properties of GC AMPARs are largely unknown, as they are absent from the soma (Silver et al., 1996a) and nonsynaptic regions of the dendrites (DiGregorio et al., 2002), we used an AMPAR model from cerebellar Purkinje cells (Wadiche and Jahr, 2001; adjusted from 33°C to 37°C) to calculate the channel response from the $[glut]_{cleft}$. We express AMPAR activation as an open probability waveform [$P_{open}(t)$]. Simulations exhibited a rapidly rising $P_{open}(t)$ when release occurred from the site opposite the central PSD, and a slow-rising $P_{open}(t)$ when this local release site failed (Figure 1C). The slow-rising $P_{open}(t)$ had a 10%–90% rise time (0.58 ms) and an amplitude, relative to the mean $P_{open}(t)$ (0.41), comparable to measured slow-rising and mean EPSC averaged across the population (Figure 1C, inset; from DiGregorio et al., 2002). It is clear from these simulations that a spillover mechanism based on rapid release from distant sites can, in principle, generate slow-rising AMPAR EPSCs at the MF-GC synapse.

Simulations of EPSCs Arising from Prolonged Local Release

To construct a model of synaptic transmission mediated by PLR of glutamate, we required a time course of release from single vesicles that could mediate slow-rising currents. Since there are no measurements of this time course for glutamatergic synapses, we estimated the $[glut]_{cleft}$ waveform from the measured slow-rising EPSC and used this waveform to derive a neurotransmitter release time course. To accomplish this, we first expressed the recorded population average slow-rising EPSC (DiGregorio et al., 2002; Figure 1C, inset) as $P_{open}(t)$ (Figure 2Ai; Experimental Procedures). We then used a least-squares optimization algorithm to search for the $[glut]_{cleft}$ waveform that, when "fed" through an AMPAR kinetic scheme, produced a $P_{open}(t)$ most similar to that underlying the measured slow-rising current (Figure 2Ai). Since the properties of the AMPARs are likely to influence the estimate of the underlying glutamate waveform, we used temperature-adjusted native AMPAR models from brain regions where they have been studied in detail: cerebellar Purkinje cells (Wadiche and Jahr, 2001; WJ), CA1 cultures (Diamond and Jahr, 1997; DJ), CA3 pyramidal neurons in hippocampal slices (Jonas et

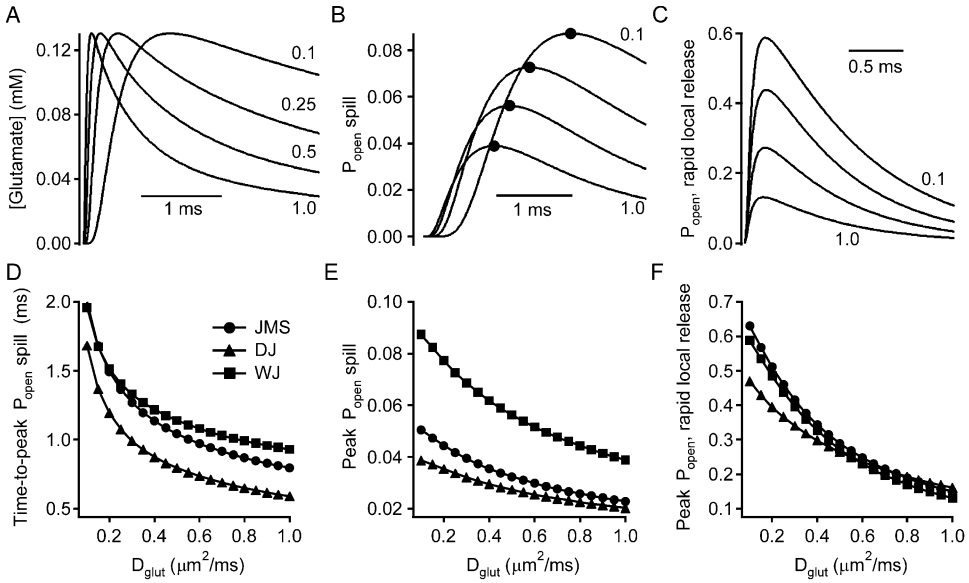

Figure 3. The Effect of Slowing Diffusion on Simulated Spillover and Rapid Local Release

(A and B) Simulated average glutamate concentration (A) and AMPAR open probability (B) [$P_{open}(t)$] for spillover using D_{glut} of 1.0, 0.5, 0.25, and 0.1 μm^2/ms and the WJ kinetic scheme. These spillover concentrations and P_{open} waveforms were calculated without release latency or stochasticity. Filled circles indicate the peak. Transients had times-to-peak of 0.93, 1.14, 1.41, and 1.96 ms, respectively.

(C) Simulated $P_{open}(t)$ for rapid local release (RLR) of 4000 molecules for the WJ scheme and D_{glut} of 1.0, 0.5, 0.25, and 0.1 μm^2/ms.

(D and E) Time-to-peak (D) and peak amplitude (E) of simulated slow-rising $P_{open}(t)$ mediated by spillover as a function of D_{glut}, for the three different kinetic schemes.

(F) Peak amplitude of $P_{open}(t)$ mediated by RLR as a function of D_{glut}; symbols as for (D).

al., 1993, Set 1; JMS), and auditory brainstem (Raman and Trussell, 1995; RT). The AMPARs underlying the RT scheme include $GluR4_{flop}$ (Ravindranathan et al., 2000), which are thought to be expressed in GCs (Mosbacher et al., 1994). These models covered the wide range of desensitization characteristics across cell types (Raman et al., 1994) and had a 4-fold range of EC_{50}. Figure 2Ai shows the best fits to the $P_{open}(t)$ of the slow-rising EPSCs using the WJ, JMS, and DJ AMPAR kinetic models (traces overlie). The $[glut]_{cleft}$ concentration derived from the three models had rapid rise times (10%–90%, 0.27–0.38 ms) and all had a similar shape and peak (116–157 μM; Figure 2Aii), with a decay that could be fit with dual exponentials with τ_1 = 0.28–0.32 ms and τ_2 = 12–45 ms. In contrast, the $P_{open}(t)$s generated with the rapidly desensitising RT kinetic scheme was unable to reproduce the slow-rising EPSCs from the MF-GC synapse (Figure 2B), and thus we did not use the RT scheme for further simulations of PLR.

Under conditions of linear diffusion, it is possible to calculate the glutamate release time course by deconvolving the $[glut]_{cleft}$ waveform underlying the slow-rising EPSC with the impulse response function (the $[glut]_{cleft}$ waveform following instantaneous local release for the MF-GC synaptic geometry; Figure 1A). Figure 2C shows the deconvolved local release time courses derived from the $[glut]_{cleft}$ waveform for the WJ kinetic scheme for three values of D_{glut}. The decay for each waveform was initially rapid (τ_1 = 0.32–0.35 ms) with a slower prolonged tail (τ_2 = 18–21 ms). These release time courses are within the range of calculated durations of emptying of small clear vesicle through a narrow fusion pore (Klyachko and Jackson, 2002). Depending on the initial value of D_{glut}, the integral of the glutamate release rate corresponds to 2.6–8.4 vesicles per EPSC (over 10 ms; WJ scheme), consistent with the observed lower relative variability of the slow-rising EPSC than the fast-rising component (DiGregorio et al., 2002). Our models of PLR and spillover demonstrate that they are both physically plausible mechanisms for the slow-rising current at the MF-GC synapse.

Simulating the Effects of Slowing Diffusion on Spillover

Since one of the key differences between currents produced by transmitter spillover and PLR is the distance over which glutamate diffuses, we investigated whether changing the mobility of glutamate could be used to distinguish between these mechanisms. Figure 3A shows a simulation of the effect of slowing diffusion on spillover-mediated $[glut]_{cleft}$. Lowering D_{glut} from 1.0 (the value in free solution) to 0.5–0.1 μm^2/ms had no effect on the peak glutamate concentration (130 μM), but slowed the time-to-peak of the $[glut]_{cleft}$ waveform by up to 997 μs (Figure 3A). The AMPAR-mediated $P_{open}(t)$ responses to these concentration waveforms (WJ kinetic scheme) are shown in Figure 3B. Lowering D_{glut} to 0.1 μm^2/ms increased the peak P_{open} by 124% and delayed the current onset, increasing the time-to-peak of spillover-mediated currents by 110%. $P_{open}(t)$ mediated by RLR also increased in amplitude when diffusion is slowed (Figure 3C) as previously predicted (Rusakov and Kullmann, 1998a) and observed (Min et al., 1998). Figure 3D shows the time-to-peak of the spillover $P_{open}(t)$ for different kinetic schemes as a function of D_{glut}. Changes in D_{glut} in the mid-to-high range led to small

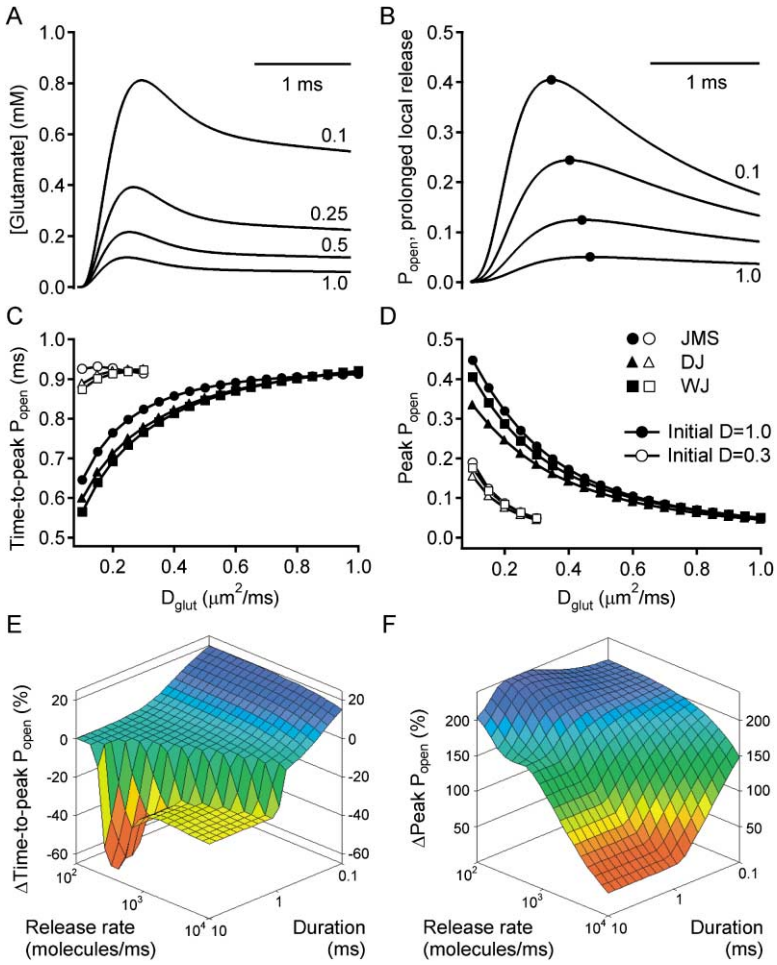

Figure 4. The Effect of Slowing Diffusion on Simulated Prolonged Local Release

(A) Simulated concentration waveforms resulting from prolonged local release (PLR) for D_{glut} of 1.0, 0.5, 0.25, and 0.1 μm^2/ms. The release time course in this panel was determined from the measured slow-rising EPSC, for an initial D_{glut} of 1.0 μm^2/ms and the WJ kinetic scheme.

(B) Open probability responses to the concentration waveforms in (A) for PLR, using the WJ kinetic scheme. Filled circles indicate peaks, with times-to-peak of 0.92, 0.85 0.73, and 0.57 ms, respectively.

(C) Time-to-peak and (D) peak amplitude of simulated slow-rising $P_{open}(t)$ mediated by PLR as a function of D_{glut}, for the three different kinetic schemes. The release time courses were determined with an initial D_{glut} of 1.0 μm^2/ms (filled symbols) and 0.3 μm^2/ms (open symbols).

(E) Relative change in the time-to-peak of $P_{open}(t)$ when lowering D_{glut} from 0.5 to 0.25 μm^2/ms for the WJ scheme. The release time courses were step-shaped of durations 0.1 to 10 ms and amplitudes 10^2–10^4 molecules/ms. The times-to-peak in this panel were measured from the beginning of glutamate release.

(F) Relative change in peak amplitude of $P_{open}(t)$ mediated by different time courses of local release, as in (E).

changes, while in the lower range, even small reductions in D_{glut} caused substantial increases in the time-to-peak. Moreover, this slowing was observed over a wide range of molecules per vesicle (2000–6000). The peak amplitude of the spillover-mediated $P_{open}(t)$, shown in Figure 3E, increased monotonically over the entire range of simulated D_{glut}. Changes in the peak AMPAR P_{open} mediated by RLR were more pronounced, increasing more steeply over the full range of D_{glut} (Figure 3F). These simulations suggest that lowering D_{glut} will increase the time-to-peak and increase the amplitude of slow-rising currents mediated by spillover.

Simulating the Effects of Slowing Diffusion on Prolonged Local Release

Figure 4A shows the effect of slowing diffusion on a $[glut]_{cleft}$ mediated by PLR. Lowering D_{glut} from 1.0 to 0.5–0.1 μm^2/ms markedly increased the amplitude of the $[glut]_{cleft}$ transients (derived with the WJ kinetic scheme) from 116 to up to 811 μM by retarding diffusion out of the cleft. However, the shape of concentration transients arising from PLR was relatively insensitive to lowering D_{glut}, with the peak slowing by only 154 μs. Figure 4B shows that the large amplitude increases are also preserved in the AMPAR responses, with the peak amplitude increasing by up to 707%. In contrast to spillover, the time-to-peak of the $P_{open}(t)$ *decreased* by 39% when D_{glut} was lowered, due to the concentration dependence of the AMPAR response rise time. This decrease in the time-to-peak (Figure 4C) and the increase in the peak P_{open} (Figure 4D) were observed consistently when lowering D_{glut} from 1.0 μm^2/ms. Since our estimate of the release time course depends on the initial D_{glut}, we repeated these simulations with initial D_{glut} values of 0.2, 0.3 (Figures 4C and 4D, open symbols), and 0.5 μm^2/ms. In general, these simulations showed that the time-to-peak decreased and the amplitude increased as above. However, some simulations with an initial D_{glut} of 0.2 or 0.3 μm^2/ms exhibited a small increase in the time-to-peak (<5%). Under these low initial D_{glut} conditions, amplitude increases were still 100%–200% for a 50% reduction in D_{glut}. We also verified that calculating $P_{open}(t)$ in our model by averaging $[glut]_{cleft}$ over the PSD did not mask an increase in the time-to-peak (Experimental Procedures). These simulations suggest that in contrast to spillover, lowering D_{glut} will generally decrease the time-to-peak of slow-rising currents mediated by PLR. However, in those cases where the time-to-peak is slightly increased by lowering D_{glut}, the peak amplitude of these currents will be increased dramatically.

To test a wider range of conditions, we examined the effect of lowering D_{glut} on release waveforms of different durations and amplitudes. Figure 4E shows a 3D plot of the relationship between the change in the time-to-

peak of $P_{open}(t)$ generated with step-shaped release events of different duration (0.1–10 ms) and release rate (10^2–10^4 molecules/ms) for the WJ model. These simulations covered a wide range of peak P_{open} values (10^{-6}–0.34). As for the simulations above, the time-to-peak of currents mediated by PLR usually remained the same or decreased on lowering D_{glut} from 0.5 to 0.25 μm^2/ms. As the release time course becomes brief (<1 ms), the time-to-peak began to increase when lowering D_{glut}. In those cases where the time-to-peak increased more than 5%, large increases (>100%) in the peak amplitude were again observed (Figure 4F). Moreover, their initial time-to-peak is rapid (>2-fold faster than slow-rising currents in the GC).

Our simulations of spillover and prolonged release show that lowering D_{glut} has different effects on the time-to-peak and amplitude of slow-rising EPSCs arising from these two mechanisms. Agents that lower glutamate mobility can therefore be used to determine whether spillover or PLR underlie slow-rising currents under a wide range of physiologically plausible conditions.

Slowing Diffusion at the Mossy Fiber-Granule Cell Synapse with Dextran

To examine the mechanism underlying slow-rising currents at the MF-GC synapse, we slowed glutamate diffusion by adding 1 mM (5% w/v) of the macromolecule dextran (43 kDa) to the extracellular medium while recording evoked EPSCs from GCs. This concentration of dextran more than doubles the viscosity (Min et al., 1998) but had little effect on the osmolality of the extracellular solution or the effective concentration of glutamate (Experimental Procedures). We isolated slow-rising AMPAR EPSC on the basis of rise time and fitted slow-rising currents to determine the amplitude and time-to-peak. The mean and isolated slow-rising EPSCs before and during dextran perfusion are shown in Figure 5A for a representative cell. Perfusion of dextran resulted in an increase in the time-to-peak of the isolated slow-rising EPSC (25% for this cell), with an average increase of 17.6% ± 7.1% (time-to-peak 1.35 ± 0.14 ms in control, 1.56 ± 0.17 ms in dextran; $p = 0.04$, $n = 9$; Figures 5A and 5B). The time-to-peak of the mean EPSC, which is dominated by the fast-rising component (DiGregorio et al., 2002), did not slow significantly (0.34 ± 0.04 ms in control, 0.35 ± 0.05 ms in dextran; $p = 0.56$, $n = 9$; Figure 5C). The absence of a change in time-to-peak of the mean EPSC excludes the possibility that the effect of dextran on slow-rising currents was caused by changes in filtering properties of the cell-electrode circuit or a change in the properties of the postsynaptic receptors.

In contrast to model predictions for RLR (Figures 3C and 3F), the amplitude of the fast-rising EPSC (defined in Experimental Procedures) was unaltered in the presence of dextran (−34.3 ± 9.3 pA in control, −32.1 ± 11.1 pA in dextran; $p = 0.34$, $n = 9$; Figure 5D). We also observed an increase in the failure rate of the fast-rising component (12.9% ± 1.3% in control, 25.0% ± 2.3% in dextran; $p = 0.04$, $n = 9$; Figure 5E), indicating a decrease in release probability in the presence of dextran. We therefore tested whether dextran-induced slowing of the slow-rising EPSCs could be accounted for by lowering the release probability. Figure 5F shows peak-normalized slow-rising EPSCs recorded in 2 and 1.5 mM $[Ca^{2+}]_o$. The mean EPSC peak amplitude recorded under these conditions decreased from −49.3 pA to −20.7 pA, respectively ($p < 0.001$; Figure 5F, inset). However, there

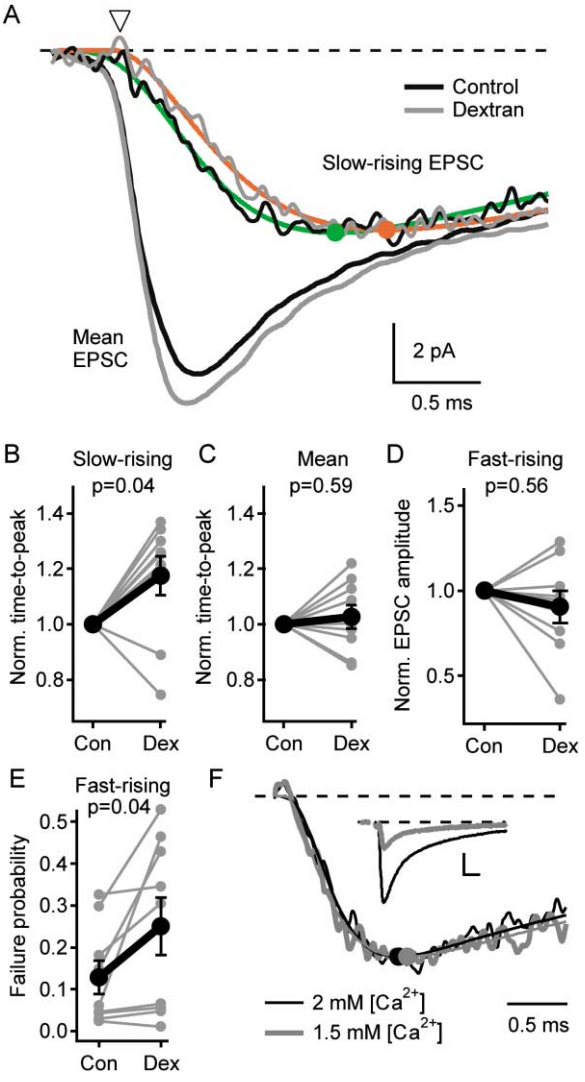

Figure 5. Dextran Application Increases the Time-to-Peak of Slow-Rising EPSCs at the MF-GC Synapse

(A) Mean AMPAR EPSC and slow-rising EPSCs recorded in control solution (black trace) and in the presence of dextran (gray trace). The traces were aligned on the 20% rise time of the mean EPSCs (open triangle). The slow-rising current was fitted with Equation 1 in control (green) and in dextran (red). Filled circles indicate the peak.

(B) Summary plot of the change in time-to-peak of the slow-rising EPSC in dextran. For (B)–(E), individual cells are indicated in gray, and average measurements are in black.

(C) Summary plot of the change in time-to-peak of the mean EPSC in dextran relative to control.

(D) Summary plot showing effect of dextran on the amplitude of the fast-rising EPSC.

(E) Summary plot showing effect of dextran on the failure probability of the fast-rising component.

(F) Normalized slow-rising EPSCs recorded in 2 and 1.25 mM $[Ca^{2+}]_o$, aligned on the 20% rise point of the mean EPSC, together with fits. Filled circles indicate peaks. Inset: mean EPSCs recorded in 2 and 1.25 mM $[Ca^{2+}]_o$; calibration bar: 10 pA, 1 ms.

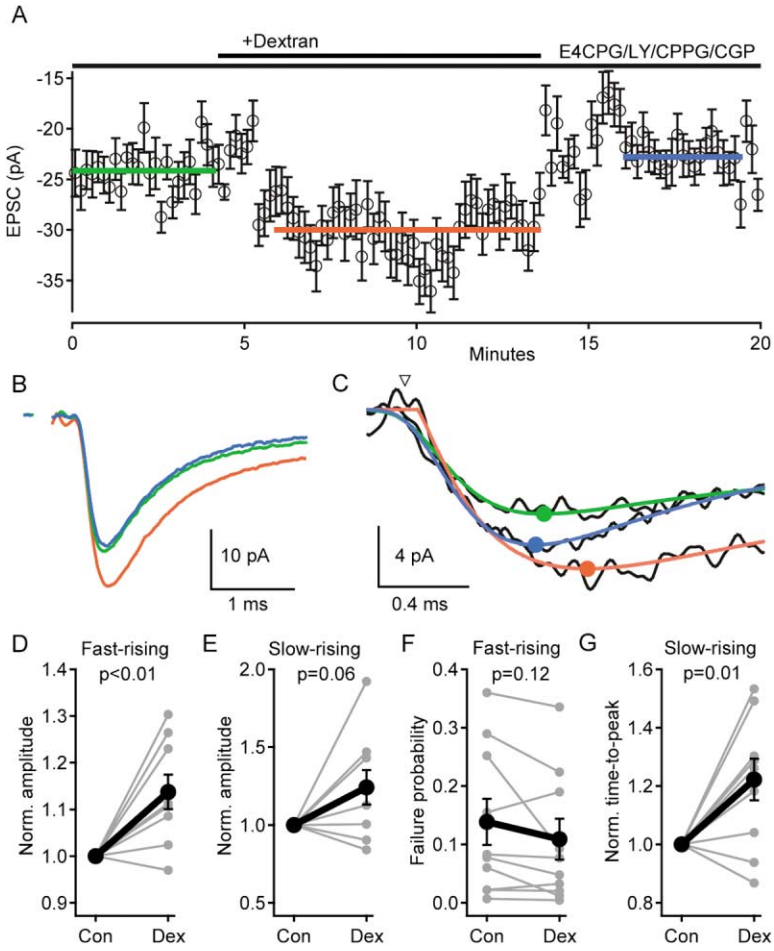

Figure 6. The Effect of Dextran on EPSCs in the Presence of Metabotropic Receptor Antagonists

(A) Running average (n = 20) of the EPSC amplitude during wash-in and wash-out of dextran for an individual cell. Abbreviations for drugs are LY341495 (LY) and CGP52432 (CGP).

(B) Mean EPSC traces before (green), during (red), and after (blue) dextran perfusion measured for periods indicated in (A).

(C) Slow-rising EPSCs measured before, during, and after dextran perfusion for same cell, fitted with Equation (1). Colors as for (B); filled circles indicate the peak. The traces were aligned on the 20% rise point of the mean EPSC (open triangle).

(D) Summary plot of the relative change in fast-rising EPSC amplitude during dextran. In (D)–(G), individual cells are indicated in gray, and average measurements are in black.

(E) Summary plot of the relative change in the amplitude of slow-rising currents in dextran.

(F) Summary plot of the failure probability in control and dextran.

(G) Summary plot of the relative change in the time-to-peak of slow-rising EPSCs in dextran.

was no change in the time-to-peak of slow-rising EPSC (1.32 ± 0.10 ms in 2 mM, 1.43 ± 0.19 in 1.5 mM $[Ca^{2+}]_o$; p = 0.42, n = 8), demonstrating that the slowing of the time-to-peak of slow-rising EPSCs in the presence of dextran is not due to a change in release probability. The slowing of the time-to-peak in these preliminary experiments is consistent with the idea that slow-rising EPSCs arise from spillover of glutamate.

Since presynaptic metabotropic receptors reduce glutamate release from MFs in cerebellum (Mitchell and Silver, 2000; T.A.N. and R.A.S., unpublished data) and the activation of presynaptic metabotropic receptors can be enhanced in dextran (Min et al., 1998), we examined whether the dextran-induced reduction in release probability could be blocked by mGluR and $GABA_B$ receptor antagonists. Figure 6A shows the time course of the effect of dextran on the amplitudes of EPSCs (running average of 20) recorded in the presence of metabotropic antagonists E4CPG, CPPG, CGP 52432, and LY 341495. Figures 6B and 6C show that in the presence of dextran, both the amplitude of the mean EPSC and the time-to-peak of the slow-rising EPSC increased by 26% in this cell and this effect was reversible. Across all cells, the amplitude of the fast-rising EPSC increased significantly with dextran in the presence of metabotropic antagonists (Figure 6D; 14% ± 4%; p = 0.006, n = 9). Although the amplitude of the slow-rising current tended to increase, this was not significant (Figure 6E; 24% ± 11%; p = 0.06, n = 9). Moreover, the failure rate of fast-rising events was unaffected by dextran in the presence of metabotropic antagonists (p = 0.12, n = 9; Figure 6F), consistent with the idea that transmitter retention in the presence of dextran reduced release probability by activating presynaptic receptors. On average, the time-to-peak of the slow-rising current was slowed by 22% ± 7% (p = 0.014, n = 9; Figure 6G), not significantly different from the slowing observed in the absence of metabotropic antagonists (p = 0.65, unpaired t test). In six cells where recordings lasted after returning to control solution, the peak amplitude of the fast-rising EPSC returned to 91% of control, significantly different from in dextran (p = 0.02). In three of four cells where long recordings were made and dextran slowed currents by more than 5%, the time-to-peak returned to at least within 5% of the control value, with an average washout of 73% for all four cells.

To examine the effect of dextran on local release in the absence of slow-rising currents, we isolated quantal successes under low release probability conditions (1 mM $[Ca^{2+}]_o$), when the chances of releasing multiple quanta per trial are small (<5%; Silver, 2003) and slow-rising currents are minimal. Figures 7Ai and 7Aii shows isolated, aligned successes recorded in 1 mM $[Ca^{2+}]_o$ control solution and in dextran, respectively. Dextran

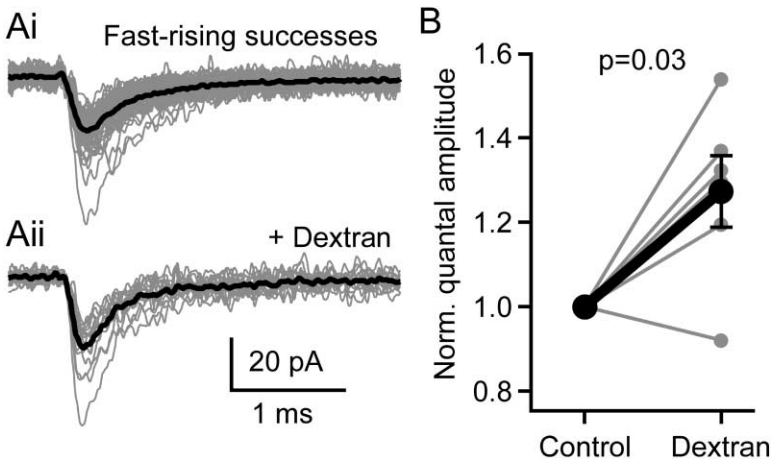

Figure 7. Dextran Increases Quantal Current Amplitude

(A) Fast-rising EPSC successes recorded in low $[Ca^{2+}]_o$ in control (Ai) and dextran (Aii), with individual currents aligned on their 10% rise time. The fraction of failures for this cell was >82% under the two conditions. In this figure, individual cells are indicated in gray, and average measurements are in black.

(B) Summary plot of the change in the mean quantal amplitude in the presence of dextran across cells.

increased the quantal amplitude by 27% ± 8% ($p = 0.02$, $n = 6$; Figure 7B) from a control value of 22.0 ± 2.9 pA, and there was no change in the failure rate (90% ± 2% in control, 93% ± 2% in dextran; $p = 0.17$, $n = 6$). The time-to-peak of quantal EPSCs did not change in dextran (191 ± 15 and 196 ± 19 μs, respectively; $p = 0.63$, $n = 6$). The potentiation was no different from that observed for the fast-rising EPSC in the presence of metabotropic blockers, suggesting that the fast-rising and slow-rising current components sum linearly at the peak of the mean EPSC ($p = 0.12$; unpaired t test). Our experimental results, which show that slow-rising currents slow by 20% in the presence of dextran, indicate that they arise from glutamate spillover from distant sites, rather than PLR of glutamate, which would predict at most a 5% increase in the time-to-peak. Moreover, dextran had little effect in the amplitude of slow-rising currents, which is also consistent with a spillover mechanism.

Estimation of D_{glut} under Control Conditions and in Dextran

Having established that spillover underlies slow-rising EPSCs, we then explored the properties of glutamate diffusion at the MF-GC synapse. Since our simulations indicate that lowering D_{glut} affects the time-to-peak of the slow-rising current and the amplitude of the RLR component differentially (Figure 8A), it was possible to make an estimate of D_{glut} under control conditions and in the presence of dextran from our experimental observations. For each initial value of D_{glut} between 0.1 and 1.0 μm^2/ms, we calculated the values of D_{glut} in dextran that reproduced the experimentally observed change in time-to-peak of the slow-rising EPSC (19.9%; $p = 0.001$, $n = 18$ pooled from experiments with and without metabotropic blockers) and increases in the fast-rising EPSC amplitude (19.2%; $p < 0.001$; $n = 15$ pooled from recordings of normal and low $[Ca^{2+}]_o$; Figure 8A). Figure 8B shows the relationship between the initial D_{glut} and the D_{glut} in dextran derived from the change in the time-to-peak of the spillover current and the change in amplitude of the RLR component for the WJ scheme. The intersection of these curves represents a unique pair of values for D_{glut} in control and dextran, where the experimentally observed changes in time-to-peak and quantal amplitude in dextran were both observed. Using this approach, we obtained values of D_{glut} in control solution of 0.23, 0.36, and 0.22 μm^2/ms for the JMS, DJ, and WJ kinetic schemes. The retardation of D_{glut} in dextran was 35%–40%. These results suggest that D_{glut} is substantially lower than in free solution.

We attempted to narrow the range of the D_{glut} estimates by taking into account the fact that some kinetic schemes better matched the measured properties of the MF-GC EPSC. To include as many possible properties of AMPARs, we predicted D_{glut}, as described above, for 12 published kinetic schemes based on fast agonist application experiments (defined in Experimental Procedures). For each scheme, we then compared the following characteristics of simulations to experimental data: the decay time course of the local component (Figure 8C; weighted over 3 ms), the time-to-peak and peak amplitude of the spillover $P_{open}(t)$ (Figures 8D and 8E), and the amplitude ratio of RLR to spillover components (Figure 8E). Simulations were carried out for each channel, at the D_{glut} estimated with that scheme, and the goodness-of-fit was assessed from the χ^2 value (Figure 8F). The mean value of D_{glut} obtained across the 12 channel models, weighted by $1/\chi^2$, gave a value for D_{glut} of 0.33 μm^2/ms and a slowing of diffusion in dextran by 36%. Our approach provides an estimate of D_{glut} that is weighted by its ability to predict the experimentally measured properties of local and spillover currents at the MF-GC synapse. Of all AMPAR schemes tested, the HR had the lowest χ^2 (Figure 8F) and gave a value of D_{glut} of 0.29 μm^2/ms. Ten of the 12 schemes, including those with the lowest χ^2, gave values of D_{glut} below 0.5 μm^2/ms (Figure 8F). We then applied the weighted mean method to calculate the error in our estimate of D_{glut} arising from the variability in our experimental data. When the change in the time-to-peak and EPSC amplitude in dextran were varied by ±1 SEM, D_{glut} ranged from 0.24 to 0.46 μm^2/ms (Figure 8B), and the reduction in D_{glut} in dextran was 30%–42%. While we cannot rule out the possibility that an uncharacterized AMPAR at the MF-GC synapse exhibits characteristics that are different from published models and gives a substantially different value of D_{glut}, our results suggest that that D_{glut} is 0.33 ± 0.13 μm^2/ms.

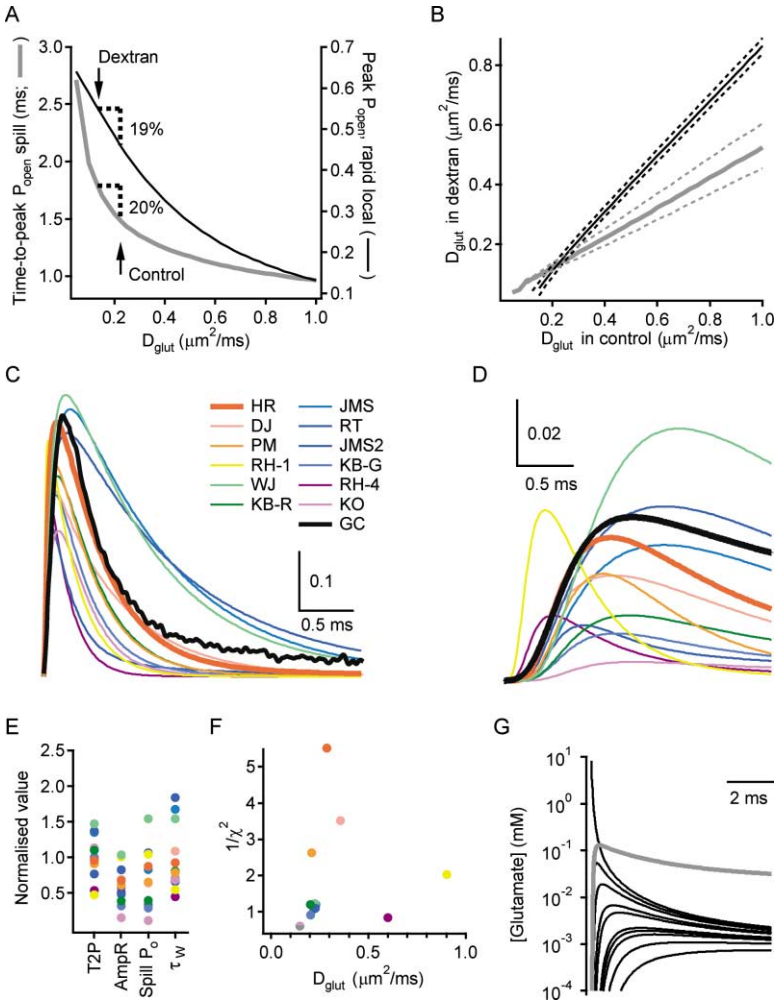

Figure 8. Estimation of the Diffusion Coefficient and the Time Course of Glutamate in the Synaptic Cleft

(A) Simulated time-to-peak of spillover (gray) and the peak amplitude of the rapid local release component (black) as a function of D_{glut} for the WJ kinetic scheme. Dotted lines indicate the locations on the curves where both the experimentally observed changes in these parameters occur for the same change in D_{glut} (arrows).

(B) Plot showing the relationship between the initial D_{glut} and the value D_{glut} in dextran required to replicate our experimental findings of 20% slowing in the time-to-peak of the slow-rising EPSC (gray) and the 19% increase in the quantal amplitude of the fast-rising EPSC (black), for the WJ kinetic scheme. Dashed lines show relationships for the experimental values ± SEM.

(C) Simulated responses to rapid local release, using the D_{glut} predicted as in (B) for each of 12 different temperature-compensated kinetic schemes. Mean quantal waveform under control conditions is expressed as P_{open} (t) (black trace).

(D) Simulated spillover P_{open}(t), as in (C), together with fit of measured population slow-rising EPSC expressed as P_{open}(t) (using Equation 1; black trace).

(E) Time-to-peak (T2P), ratio of rapid local to spillover peak P_{open} amplitudes (AmpR), peak spillover P_{open} (Spill P_o), and weighted decay of rapid local P_{open}(t) (τ_w; over 3 ms) of simulated P_{open}(t) using D_{glut} estimated for each kinetic scheme, colors as in (C), normalized to the experimentally observed value.

(F) Goodness-of-fit of values from (E), for each kinetic scheme, expressed as $1/\chi^2$, as a function of calculated D_{glut}.

(G) Simulated $[glut]_{cleft}$ from each of the ten distinct release locations (Figure 1B) in our simulations with the weighted D_{glut} of 0.33 μm^2/ms (black lines). Thick gray line shows average $[glut]_{cleft}$ produced by spillover.

To assess the accuracy of our estimate of D_{glut}, we examined how it was influenced by model parameters that are not well defined for the MF-GC synapse in P25 rats. We report both the weighted mean measure of D_{glut}, since it takes into account the possibility that the best fitting channel is different under different model conditions, and the HR scheme, which had the lowest χ^2. We first examined a range of synaptic vesicle glutamate concentrations centered on that estimated in cortex (200 ± 100 mM; Burger et al., 1989; Riveros et al., 1986; Xu-Friedman and Regehr, 2003). This value corresponds to 4000 ± 2000 molecules in a 48 nm MF vesicle (Palay and Chan-Palay, 1974; Xu-Friedman and Regehr, 2003). D_{glut} was 0.20 μm^2/ms and 0.44 μm^2/ms, for 2000 and 6000 molecules, respectively, for the weighted approach and 0.16 μm^2/ms and 0.41 μm^2/ms for the HR kinetic scheme. When we used an upper bound for the duration of acetylcholine release estimated by Stiles et al. (1996), the estimate of D_{glut} was 3% lower and 0.2% higher, respectively. We also examined the sensitivity of D_{glut} to our estimate of release probability, since it influences both the peak concentration of glutamate arising from spillover and our estimate of the peak slow-rising P_{open}. Reducing or increasing the release probability by 50% had little effect on our estimate of D_{glut}, changing it by only 6% and 4%, respectively. To account for potential changes in the intersite distance between P18 and P25 (Hamori and Somogyi, 1983), we increase the intersite distance to 0.80 μm (calculated from the change in number of synapses per MF profile). This increased D_{glut} by 18% and 14%. Electron micrographs suggest the distance between membranes in the regions between active zones is either approximately equal (Jakab and Hamori, 1988; Palay and Chan-Palay, 1974) or less (Xu-Friedman and Regehr, 2003), which may be due to fixation. We therefore simulated diffusion in a geometry where the cleft width was halved outside the active zone (to 10 nm). With this geometry, the weighted mean D_{glut} increased to 0.43 and 0.50 μm^2/ms. Finally, adding 200 glutamate binding sites (Robert and Howe, 2003) per active zone to mimic glutamate buffering by AMPARs had little effect on the estimated D_{glut}, giving 1.7% and 0.2% increases for the weighted mean and HR model, respectively. These simulations of uncertainties in model parameters suggest that D_{glut} is between 2- and 5-fold lower than free solution.

The Concentration of Glutamate in the Synaptic Cleft

Having estimated D_{glut}, we calculated the components underlying the mean spillover $[glut]_{cleft}$ waveform. Figure 8G shows individual concentration waveforms from each of the ten distinct release locations shown in Figure 1B, which had different amplitudes and rise times but converged at late times. In the absence of local release, the average spillover concentration (i.e., the sum of all individual transients scaled by the release probability and convolved with the latency distribution) reached 129 μM and had a 10%–90% rise time of 198 μs. These values are comparable to those obtained by fitting the experimentally measured slow-rising current (Figure 2Aii). Its decay could be approximated with a dual exponential function with $\tau_1 = 1.47$ ms (67%) and $\tau_2 = 13.3$ ms (33%). Comparison of the $[glut]_{cleft}$ waveforms arising from individual release sites with the average response (Figure 8G) shows that the rise and peak of the spillover waveform is determined predominantly by a few close sites. In contrast, the slow decay of the $[glut]_{cleft}$ waveform is determined by the summation of glutamate from many, more remote sites. Our prediction of $[glut]_{cleft}$ arising from spillover will be least accurate at late times, because glutamate uptake (DiGregorio et al., 2002) and sites more remote than those we have simulated may contribute to the waveform.

Discussion

We examined the properties of release underlying slow-rising AMPAR-mediated EPSCs at the cerebellar MF-GC synapse. Our simulations show that prolonged local release and transmitter spillover can be distinguished on the basis of changes in the time course and amplitude of AMPAR-mediated slow-rising currents when the glutamate diffusion is slowed. We have used the macromolecule dextran to slow diffusion in cerebellar slices and examined changes in EPSCs. Our results indicate that transmitter spillover, rather than PLR, underlies the slow-rising AMPA EPSC at the MF-GC synapse. Moreover, our results provide an experimental estimate of the diffusion coefficient of glutamate in the synaptic cleft and suggest that it is approximately one third of the value in free solution at physiological temperature.

The Use of Dextran for Distinguishing Prolonged Local and Distant Transmitter Release

Our approach for separating local release from distant release relies on slowing glutamate diffusion in the synaptic cleft. A reduction in D_{glut} slows the $[glut]_{cleft}$ waveform arising from distant sites and the time-to-peak of $P_{open}(t)$ mediated by spillover but has little effect on the time-to-peak of $P_{open}(t)$ generated by PLR because of the short distances over which glutamate diffuses within the active zone. Reducing D_{glut} does, however, substantially enhance the accumulation of locally released glutamate by slowing diffusion out of the cleft, leading to a substantial enhancement of the peak $[glut]_{cleft}$. In our simulations, changing D_{glut} has little effect on the shape of the $[glut]_{cleft}$ waveform mediated by PLR, because it is dominated by the release time course. In contrast, the peak $[glut]_{cleft}$ resulting from spillover is independent of D_{glut}. The modest increases in the predicted peak P_{open} of spillover responses on lowering D_{glut} result from the slower $[glut]_{cleft}$ waveform, which enhances receptor activation. It should be noted that at short intersite distances the dextran-induced slowing will be small, and may be comparable to the speeding due to channel kinetics and therefore would be difficult to distinguish spillover from PLR.

Our approach assumes that dextran does not slow the rate of diffusion within the fusion pore, as this would increase the time-to-peak of the postsynaptic current. This is unlikely given dextran is an inert macromolecule and that its hydrodynamic radius (7.3 nm) (Nicholson and Tao, 1993) is much larger than the estimated fusion pore radius for microvesicles in kiss-and-run release mode (0.3 nm) (Klyachko and Jackson, 2002). It is possible that dextran could interact with pores with larger diameters. However, the fact that we did not observe a slowing of quantal currents argues against this possibility. Our method also assumes that dextran does not affect the volume of the extracellular space. If, as a result of dextran perfusion, the distance between pre- and postsynaptic membranes decreased, the amplitude of the RLR response should increase as observed experimentally. However, simulations show that halving the distance between pre- and postsynaptic membranes outside the active zone *decreased* the time-to-peak of the slow-rising current by 4% and thus cannot account for our results.

The use of dextran for distinguishing PLR from spillover provides a new tool for investigating the mechanisms underlying transmission and transmitter diffusion synapses where rise times can be reliably measured. In general, a ~35% change in D_{glut} in dextran would produce at least a 13% slowing (Figure 3E) in the time-to-peak in our simulations if the currents are mediated by spillover, and a greater than 70% increase (Figure 4D) in the peak amplitude of slow-rising currents mediated by PLR. Any decrease in the time-to-peak of the slow-rising current upon lowering D_{glut} indicates the presence of a PLR mechanism (Figure 4E), and under most conditions this would be associated with a substantial potentiation in the peak amplitude. Indeed, it should also be possible to use this method to examine the mechanisms underlying transmission before and after LTP at hippocampal synapses (Choi et al., 2000).

Glutamate Release from Vesicles at Central Synapses

Our results suggest that both fast and slow-rising EPSCs at the MF-GC synapse arise from rapid release at various distances from the postsynaptic receptors. Such rapid release could occur through a fusion pore and/or full vesicle fusion. Although it is possible that some vesicular release could be ectopic (i.e., between active zones; Matsui and Jahr, 2003), reproduction of spillover currents with our model of the MF-GC synapse demonstrates that rapid release restricted to the center of active zones is sufficient to account for our experimental data. If release events mediated by narrow fusion pores are present, they occur infrequently, as reported for neurosecretary cells (~5%; Klyachko and Jackson, 2002), and therefore contribute little to transmission at

this synapse. At hippocampal synapses, it is possible that neurotransmitter release via rate-limiting, narrow fusion pores is more prevalent (Choi et al., 2000; Renger et al., 2001). Indeed, such a release mode may be a developmental phenomenon (Renger et al., 2001), which disappears once rapid synaptic communication via AMPARs is established.

Why Is Spillover So Prominent at the MF-GC Synapse?

Some theoretical studies of glutamate diffusion into the three-dimensional hippocampal neuropil suggest that glutamate is not likely to activate low-affinity receptors at neighboring synapses (Barbour, 2001; Franks et al., 2002). However, when diffusion within a planar space with no sinks is simulated, neighboring PSDs are strongly activated (Otis et al., 1996; Xu-Friedman and Regehr, 2003). We compared the peak glutamate concentration attained from the distant release of a single vesicle in our geometry with predictions from previous modeling studies, accounting for differences in vesicular content, intersite distance, and release time course. Compared to simulations of the $[glut]_{cleft}$ for MF-GC geometry, a planar geometry produced a 51% greater peak concentration (Holmes, 1995), while a 3D model of parallel fiber synapses incorporating the porous neuropil (Rusakov, 2001) produced a concentration 5-fold lower than that at the MF-GC synapse. Simulations of spillover currents in hippocampus (Barbour, 2001) were 9-fold smaller than for simulations with our geometry with the same kinetic scheme and D_{glut}. It is therefore likely that the MF-GC synaptic morphology, which is intermediate between a planar geometry and those used for simulating synapses on spines, contributes to prominent spillover. The large number of active zones per terminal ($\sim$191–440; Xu-Friedman and Regehr, 2003) and the inability of glutamate transporters to remove glutamate from the cleft on the millisecond timescale (DiGregorio et al., 2002) also contribute to prominent glutamate spillover. In situ hybridization studies have suggested that mRNA for $GluR4_{flop}$ subunits, which confer fast desensitization properties, are expressed in GCs (Mosbacher et al., 1994), consistent with the rapid time course of the EPSC (Silver et al., 1992). However, our finding that kinetic schemes with rapidly desensitizing properties cannot reproduce the spillover waveform except at very low occupancies ($\sim$5-fold lower than measured) suggest that GCs have AMPARs with less profound desensitization. These properties may allow glutamate spillover to activate AMPARs even following RLR.

Limitations in Estimating D_{glut}

Our approach for estimating D_{glut}, which involves a perturbation of glutamate diffusion in the cleft, relies on quantification of both the synaptic currents and the anatomy of the MF-GC synapse.

Uncertainties in our estimate of D_{glut} arise largely from the AMPAR model, the number of molecules per vesicle, the intersite distance, and the experimental error. These parameters affect the estimate of D_{glut} because they alter the sensitivity of either the occupancy of the RLR response or the time-to-peak of spillover $P_{open}(t)$, to changes in D_{glut}. The $[glut]_{cleft}$ arising from RLR is governed by diffusion out of the active zone, while spillover is determined predominantly by diffusion between active zones. Our estimation of D_{glut} in the synaptic cleft therefore assumes that the diffusion coefficient in these two regions is similar. Since it is unknown whether this assumption is accurate, we examined how differences in D_{glut} inside and outside the active zone affected our estimate of D_{glut}. Simulations of nonuniform glutamate diffusion where D_{glut} in the active zone was set to between 75% and 25% of the D_{glut} in regions between active zones show that diffusion in the perisynaptic region must be less than free solution in order to get our estimate of D_{glut} (data not shown). Moreover, they suggest that our method provides a value of D_{glut} that is approximately midway between the D_{glut} values within and between active zones.

Neurotransmitter Diffusion in the Synaptic Cleft

Our finding that glutamate diffusion in the synaptic cleft is substantially slower than in free solution is consistent with previous estimates of the retardation of glycine (4-fold) (Faber et al., 1985) and acetylcholine (1.5-fold) (Land et al., 1984) diffusion in the synaptic cleft based on simulations predicting the time course of quantal conductance changes. Moreover, our estimate of the slowing of glutamate diffusion by adding 5% dextran is 30%–42%, consistent with theoretical estimates based on the radius of dextran (Nicholson and Tao, 1993), which predicted a 27%–50% retardation of transmitter diffusion (Min et al., 1998; Perrais and Ropert, 2000), and with the 20%–30% retardation predicted from NMR studies of water self-diffusion in dextran (Rusakov and Fine, 2003; Watanabe et al., 1996). The difference between our estimate of D_{glut} at the MF-GC synapse and that in free solution is not due to geometric tortuosity (Nicholson and Sykova, 1998), since the intersite distance used in our model was measured along the surface of the presynaptic membrane (Xu-Friedman and Regehr, 2003), and we model diffusional sinks between neighboring dendrites, thus explicitly accounting for the full path length of diffusion. Previous measurements have shown that the bulk tissue tortuosity (λ) in the GC layer of the cerebellum is 1.77 (Rice et al., 1993), corresponding to an apparent diffusion coefficient 3-fold less than for aqueous solution. This includes macroscopic geometrical factors such as diffusion around cells, which account for a slowing of 1.5 fold ($\lambda = 1.225$) (Hrabetova et al., 2003), leaving a 2-fold slowing by microscopic factors including D_{glut}. If the diffusion properties of the extracellular space are similar to those in the synapse, this value is consistent with our upper estimate for D_{glut}. However, our mean value for D_{glut} of 0.33 μm^2/ms suggests that diffusion is slower in the glomerulus than in the surrounding extracellular space, which may comprise the majority of the extracellular volume in the GC layer. Although the mechanisms underlying glutamate mobility in the synapse are unknown, it is possible that macromolecules, such as ion channels and constituents of the extracellular matrix, contribute to slowing glutamate diffusion (Syková, 2001). However, diffusion could also be slowed by an unidentified glutamate binding protein that has a much greater capacity than AMPARs and transporters. Under these conditions, our estimate

of D_{glut} would reflect an effective diffusion coefficient (but see Barbour, 2001).

Impact of a Low D_{glut} on Synaptic Transmission

A low D_{glut} has implications for the independent operation of neighboring synaptic contacts, since the $[glut]_{cleft}$ waveform mediated by spillover slows as D_{glut} is lowered without a decrement in the amplitude. Our results show that this produces a larger spillover-mediated postsynaptic activation than would be expected for diffusion in free solution. In addition, a low D_{glut} may enhance the ability of spillover to induce AMPAR desensitization and thus will influence short-term synaptic plasticity (Xu-Friedman and Regehr, 2003). A D_{glut} that is lower than in free solution will also produce a slower transmitter concentration waveform following RLR (Franks et al., 2002; Rusakov and Kullmann, 1998a). This will increase the occupancy of the postsynaptic receptors and thus the amplitude of synaptic current. At the MF-GC synapse, we found no significant difference in the time-to-peak or decay time constants of quantal currents in control and dextran (data not shown), indicating that the shape of the quantal current is relatively insensitive to D_{glut}. These results together with our diffusion model suggest that the decay of $[glut]_{cleft}$ is faster than the decay of the quantal current. A diffusion coefficient substantially below free solution could therefore allow this synapse to operate with fewer molecules per vesicle, without compromising the rapid kinetics associated with low-affinity receptors. Our results indicate that slowing diffusion with dextran enhances synaptic currents and the activation of presynaptic metabotropic receptors. The mobility of neurotransmitters is therefore an important determinant of both pre- and postsynaptic efficacy.

Experimental Procedures

Electrophysiological Recordings

Parasagittal slices of the vermal cerebellum were prepared from 25-day-old Sprague-Dawley rats as previously described (Silver et al., 1996b) except for the slicing solution, which contained 85 mM NaCl, 2.5 mM KCl, 1.25 mM NaH_2PO_4, 25 mM $NaHCO_3$, 25 mM glucose, 63 mM sucrose, 0.5 mM $CaCl_2$, 4 mM $MgCl_2$, and 0.5 mM ascorbic acid. After 30 min incubation at 32°C, the slices were transferred to recording solution (125 mM NaCl, 2.5 mM KCl, 1.25 mM NaH_2PO_4, 26 mM $NaHCO_3$, 25 mM glucose, 2 mM $CaCl_2$, 1 mM $MgCl_2$) with 1 mM kynurenic acid and 0.4 mM ascorbic acid added and stored at room temperature. Fire-polished patch electrodes were filled with one of two solutions: (1) 110 mM $KMeSO_4$, 40 mM HEPES, 4 mM NaCl, 5 mM EGTA, 1.78 mM $CaCl_2$, 0.3 mM NaGTP, and 4 VMgATP (pH 7.3), or (2) as (1) except with 1 mM KCl, 0.5 mM EGTA, and no $CaCl_2$. Electrode tip resistances were 6–10 MΩ. Recordings were made with 10 μM AP5, 20 μM 7-chlorokynurenic acid, 10 μM SR-95531 (Tocris), and 0.5 μM strychnine (Sigma) at 36°C–37°C and −70 mV. Recording solutions with 1 and 1.25 mM $[Ca^{2+}]_o$ contained 3 and 3.67 mM $[Mg^{2+}]_o$, and the osmolarity was adjusted with glucose. Metabotropic receptor antagonists E4CPG (20 μM), CPPG (20 μM), CGP 52432 (2 μM), and LY 341495 (2 μM) were obtained from Tocris. Synaptic currents were evoked by extracellular stimulation of MFs at 0.5–5 Hz and recorded with an Axopatch 200B amplifier and Axograph 4 or Neuromatic software. Currents were filtered to 7.1 kHz, and digitized at 100 kHz. Cells were excluded if the leak current exceeded −50 pA, if the series resistance was larger than 35 MΩ, or the filter frequency from the cell-electrode circuit changed by more than 25%.

43 kDa dextran (Sigma; 50 g/L, 1 mM) was added when specified. This had little effect on the osmolality of the extracellular solution (1.1%; consistent with Parsegian et al., 1995) as measured with a vapor pressure osmometer (Wescor) and is therefore unlikely to change the extracellular volume fraction of the tissue. However, dextran has been proposed to reduce the volume fraction of the free solution due to molecular overcrowding (Perrais and Ropert, 2000; Rusakov and Kullmann, 1998b). We therefore tested whether the effective concentration of glutamate was affected by dextran by comparing the change in osmolality when 10 mM Na-glutamate was added to control solutions and to solutions containing dextran. The absence of any significant difference in the change in osmolality with the addition of Na-glutamate (11.6 ± 2.4 and 11.6 ± 3.4 mOsm, respectively, mean ± SD, n = 5–8 for each measurement; $p>0.95$, unpaired t test) suggests that the activity of glutamate is unaffected by dextran. Recording solution was perfused using a Gilson Minipuls 3 peristaltic pump to ensure constant flow independent of viscosity. Temperature changes during solution change (up to 3°C) were compensated prior to the measurement period. Dextran was perfused for 5–20 min before recordings to allow for equilibration or for sufficient time for the amplitude to reach steady state (where $\tau_{onset} \approx$ 1.5 min). The recording and stimulating electrodes were adjusted according to landmarks on the surface of the slice to compensate for transient slice movement, which occurred occasionally during the application of dextran as reported previously (Perrais and Ropert, 2000; Rusakov and Kullmann, 1998b).

Analysis of Synaptic Currents and Estimation of the Glutamate Concentration Waveform

Synaptic recordings were analyzed within the Igor Pro environment (WaveMetrics) using Neuromatic (http://www.physiol.ucl.ac.uk/research/silver_a/). Analysis was restricted to time-stable events (Silver et al., 1996b) and individual traces were filtered to 3.3 kHz using a Gaussian filter. Slow-rising EPSCs were identified as described by DiGregorio et al. (2002). Briefly, after stimulus artifact subtraction using subthreshold recordings or extrapolation from exponential fits, EPSC successes were identified on the basis of being at least 3–5 SDs above background noise over a 1 ms window. 20%–80% or 10%–90% rise times were measured from individual currents. EPSCs were considered as slow-rising if they were synaptic failures, or if their rise time was more than 5 SD above the mean of a Gaussian fit to the rise time distribution, and if the peak derivative of the EPSC was less than 60–100 pA/ms (after 2.5 kHz filtering). The mean EPSC and mean $P_{open}(t)$ are defined as the average of all stimuli including failures and slow-rising events. In this study, the fast-rising EPSC and fast-rising $P_{open}(t)$ are defined as the mean EPSC minus the slow-rising EPSC and the mean $P_{open}(t)$ minus the slow-rising $P_{open}(t)$, respectively. For the measurement of quantal amplitude, the artifact was removed by subtracting the averaged slow-rising (mostly failures) trace from all the traces. The failure probability of the fast-rising component was calculated as the ratio of failures plus slow-rising successes to the overall number of stimuli. To improve the estimate of the time-to-peak and amplitude of slow-rising currents, we fitted them with the following equation (derived from Bekkers and Stevens, 1996):

$$EPSC(t) = A_1\left(1 - \exp\left(-\frac{t - t_0}{\tau_{rise}}\right)\right)^n \left(A_2 \exp\left(-\frac{t - t_0}{\tau_{decay1}}\right) + (1 - A_2)\exp\left(-\frac{t - t_0}{\tau_{decay2}}\right)\right). \quad (1)$$

The time-to-peak of the slow-rising current was measured as the time from the 20% rise time of the mean EPSC to the peak of the fitted slow-rising EPSC.

The population slow-rising EPSC (Figure 1C, inset; from DiGregorio et al., 2002) was converted to $P_{open}(t)$ by scaling the peak of the waveform to

$$P_{open}(t_2) = \frac{P_R\, P_{QAMPA}\, L_Q\, EPSC_{slow}(t_2)}{EPSC_{fast}\,(t_1)}, \quad (2)$$

where P_R is the quantal release probability (0.46), which was determined with spillover-corrected multiple-probability fluctuation analysis, L_Q (0.84) is the ratio of stimulus aligned and rise-aligned quantal currents (P. Sargent, D.A.D., T.A.N., and R.A.S., unpublished data), and P_{QAMPA} is the AMPA channel open probability at the peak of a quantal EPSC (0.45) (Silver et al., 1996b). $EPSC_{fast}$ is the amplitude of the fast-rising EPSC, and $EPSC_{slow}$ is the amplitude of the slow-

rising EPSC, where (t_1) refers to the time of the peak of the fast-rising EPSC and (t_2) to the peak of the slow-rising EPSC (DiGregorio et al., 2002). This gave a P_{open} of 0.05 and assumes slow-rising and fast-rising currents summate linearly (see Results) (P. Sargent, D.A.D., T.A.N., and R.A.S., unpublished data). To find the $[glut]_{cleft}$ underlying the measured $P_{open}(t)$, 100 equally spaced points over 10 ms were optimized in amplitude using the Levenberg-Marquardt routine (Igor Pro). If this method did not converge, we used a stochastic search algorithm and an equation similar to (1) for $[glut]_{cleft}$. Values are stated as mean ± SEM, error bars denote the SEM, and all statistical tests were done with Student's paired two-tailed t test unless stated otherwise.

Cleft Glutamate Concentration Simulations

The glutamate concentration transients were numerically integrated using an explicit finite-difference method similar to that described by Crank (1975), using voxels of side length $dx = 0.02$ or 0.01 μm. We defined the geometry with a binary three-dimensional matrix, S, where $S_{i,j,k}$ is 1 if the voxel at (i, j, k) is in extracellular space, and 0 if it is impermeable. We imposed zero flux across surfaces between extracellular and impermeable voxels with the following finite-difference scheme:

$$C'_{i,j,k} = C_{i,j,k} + \frac{dt \cdot D_{glut}}{dx^2} \times \left(\begin{array}{c} S_{i+1,j,k}C_{i+1,j,k} + S_{i-1,j,k}C_{i-1,j,k} + S_{i,j+1,k}C_{i,j+1,k} + \\ S_{i,j-1,k}C_{i,j,-1,k} + S_{i,j,k+1}C_{i,j,k+1} + S_{i,j,k-1}C_{i,j,k-1} - SC_{i,j,k} \end{array} \right), \quad (3)$$

where

$$S = S_{i+1,j,k} + S_{i-1,j,k} + S_{i,j+1,k} + S_{i,j-1,k} + S_{i,j,k+1} + S_{i,j,k-1} \quad (4)$$

and dt is the time step, D_{glut} the diffusion coefficient for glutamate, and C and C' the glutamate concentrations at the previous and current time-step, respectively. The time step dt was set to

$$dt = \frac{0.4 \cdot dx^2}{3 \cdot D_{glut}}, \quad (5)$$

which is the solution to equation 8.50 from (Crank, 1975) for a stability restriction of 0.4. This was determined as follows: The total error, i.e., the combination of round off and truncation errors, as a function of dt, has a U-shaped form (Boyce and DiPrima, 1986), and this shape was replicated in the amplitude of the $[glut]_{cleft}$ at a particular time point. A stability restriction of 0.4 gave a minimal total error. Typical values of dt were 0.053–1.1 μs. Total glutamate was monitored during the simulation to ensure against unidentified losses. We verified that diffusion within our synaptic geometry was not affected by the presence of sealed boundaries by extending the boundaries in x, y, and z dimensions until there was no further change (<1%) in the time-to-peak and amplitude of the spillover $P_{open}(t)$ with $D_{glut} = 1.0$ μm²/ms, where equilibration is the fastest. For simulations with inhomogeneous D_{glut}, the glutamate concentration was determined by calculating the glutamate flux between voxels according to Fick's first law as previously described (Rusakov, 2001). This method gave the same result as the explicit finite-difference approach when D_{glut} was uniform. Buffering of glutamate due to fixed buffers was calculated with Euler integration at each time step. As diffusion in this case is not linear, the average spillover concentration was approximated by simultaneous release of 4000 × 0.46 molecules at each distant release site and $[glut]_{cleft}$ calculated at a central PSD. Deconvolution was performed using a fast Fourier transform.

Simulation of Synaptic Currents and Estimation of D_{glut}

The Igor Pro random number generator was used to identify active sites and to choose latencies according to the measured release latency distribution for quantal release from a single release site at this preparation (normal with $\sigma = 54$ μs at 37°C; P. Sargent, D.A.D., T.A.N. and R.A.S., unpublished data). In the simulations where spillover was compared to PLR, latency and stochastic release was omitted since for the latter mechanism it was not possible to calculate these parameters. For the estimation of D_{glut}, simulated spillover concentrations were convolved with the latency distribution. Moreover, for calculation of the amplitude ratio, the RLR $P_{open}(t)$ were scaled by the release probability and convolved with the latency distribution. The simulated amplitude ratio was compared to the population average ratio (DiGregorio et al., 2002), which was corrected for the contribution of slow-rising currents to the peak of the mean EPSC. The current responses of AMPAR kinetic schemes to simulated concentration transients for individual trials were computed with Euler or 4th order Runge-Kutta integration. To match recording conditions, we adjusted published rate constants with a Q_{10} of 2 (Silver et al., 1996a), and 1.25 for the glutamate binding rates, which may be diffusion limited. Temperature correcting in this manner alters the affinity for glutamate. Application of a uniform Q_{10} of 2 gave a weighted D_{glut} of 0.44 μm²/ms. A Q_{10} for diffusion of 1.25 was determined from the temperature dependence of limiting equivalent conductivities for a number of different cations and anions using the Nernst-Hartley equation (Robinson and Stokes, 2002). A similar value was obtained from the temperature dependence of the viscosity of water using the Stokes-Einstein equation (Robinson and Stokes, 2002). AMPAR schemes not defined in the results are: JMS2 (Jonas et al., 1993; set 2), KB-G and KB-R (Krampfl et al., 2002), PM (Partin et al., 1996), RH-1 and RH-4 (Robert and Howe, 2003; their Figure 3). Time-to-peak of simulated concentrations and currents were calculated in a similar manner to GC EPSCs.

We examined whether local concentration gradients within the PSD were important in changing the time-to-peak of slow-rising currents mediated by PLR by dividing the PSD into six concentric circles and calculating AMPAR $P_{open}(t)$ for each separate concentric circle. We found little difference in the effect of lowering D_{glut} compared to simulations of PLR in which we averaged [glut] over the PSD, and a small impact on the estimate of D_{glut} (5.2% increase for HR scheme).

Acknowledgments

This work was supported by the Wellcome Trust, E.U., and the MRC. R.A.S. is in receipt of a Wellcome Trust Senior Fellowship. T.A.N. is supported by the Wellcome Trust graduate program. We thank W. Regehr for providing the deconvolution algorithm and J. Clements for acquisition software, D. Kullmann, A. Roth, and D. Rusakov for helpful discussions during the project, and D. Attwell, B. Barbour, L. Cathala, D. Kullmann, A. Roth, D. Rusakov, C. Saviane, and V. Steuber for comments on the manuscript.

Received: October 20, 2003
Revised: March 19, 2004
Accepted: April 28, 2004
Published: June 9, 2004

References

Aravanis, A.M., Pyle, J.L., and Tsien, R.W. (2003). Single synaptic vesicles fusing transiently and successively without loss of identity. Nature *423*, 643–647.

Barbour, B. (2001). An evaluation of synapse independence. J. Neurosci. *21*, 7969–7984.

Bekkers, J.M., and Stevens, C.F. (1996). Cable properties of cultured hippocampal neurons determined from sucrose-evoked miniature EPSCs. J. Neurophysiol. *75*, 1250–1255.

Boyce, W.E., and DiPrima, R.C. (1986). Elementary Differential Equations, 4th Edition (New York: John Wiley & Sons)

Burger, P.M., Mehl, E., Cameron, P.L., Maycox, P.R., Baumert, M., Lottspeich, F., De Camilli, P., and Jahn, R. (1989). Synaptic vesicles immunoisolated from rat cerebral cortex contain high levels of glutamate. Neuron *3*, 715–720.

Carter, A.G., and Regehr, W.G. (2000). Prolonged synaptic currents and glutamate spillover at the parallel fiber to stellate cell synapse. J. Neurosci. *20*, 4423–4434.

Cathala, L., Brickley, S., Cull-Candy, S., and Farrant, M. (2003). Maturation of EPSCs and intrinsic membrane properties enhances precision at a cerebellar synapse. J. Neurosci. *23*, 6074–6085.

Chaudhry, F.A., Lehre, K.P., van Lookeren Campagne, M., Ottersen, O.P., Danbolt, N.C., and Storm-Mathisen, J. (1995). Glutamate trans-

porters in glial plasma membranes: highly differentiated localizations revealed by quantitative ultrastructural immunocytochemistry. Neuron *15*, 711–720.

Choi, S., Klingauf, J., and Tsien, R.W. (2000). Postfusional regulation of cleft glutamate concentration during LTP at 'silent synapses'. Nat. Neurosci. *3*, 330–336.

Choi, S., Klingauf, J., and Tsien, R.W. (2003). Fusion pore modulation as a presynaptic mechanism contributing to expression of long-term potentiation. Philos. Trans. R. Soc. Lond. B Biol. Sci. *358*, 695–705.

Clements, J.D. (1996). Transmitter timecourse in the synaptic cleft: its role in central synaptic function. Trends Neurosci. *19*, 163–171.

Crank, J. (1975). The Mathematics of Diffusion, 2nd Edition (Oxford, UK: Clarendon Press).

Diamond, J.S., and Jahr, C.E. (1997). Transporters buffer synaptically released glutamate on a submillisecond time scale. J. Neurosci. *17*, 4672–4687.

DiGregorio, D.A., Nusser, Z., and Silver, R.A. (2002). Spillover of glutamate onto synaptic AMPA receptors enhances fast transmission at a cerebellar synapse. Neuron *35*, 521–533.

Faber, D.S., Funch, P.G., and Korn, H. (1985). Evidence that receptors mediating central synaptic potentials extend beyond the postsynaptic density. Proc. Natl. Acad. Sci. USA *82*, 3504–3508.

Finkel, A.S., and Redman, S.J. (1983). The synaptic current evoked in cat spinal motoneurones by impulses in single group 1a axons. J. Physiol. *342*, 615–632.

Forti, L., Bossi, M., Bergamaschi, A., Villa, A., and Malgaroli, A. (1997). Loose-patch recordings of single quanta at individual hippocampal synapses. Nature *388*, 874–878.

Franks, K.M., Bartol, T.M., Jr., and Sejnowski, T.J. (2002). A Monte Carlo model reveals independent signaling at central glutamatergic synapses. Biophys. J. *83*, 2333–2348.

Galarreta, M., and Hestrin, S. (2001). Spike transmission and synchrony detection in networks of GABAergic interneurons. Science *292*, 2295–2299.

Gandhi, S.P., and Stevens, C.F. (2003). Three modes of synaptic vesicular recycling revealed by single-vesicle imaging. Nature *423*, 607–613.

Geiger, J.R., Lubke, J., Roth, A., Frotscher, M., and Jonas, P. (1997). Submillisecond AMPA receptor-mediated signaling at a principal neuron- interneuron synapse. Neuron *18*, 1009–1023.

Hamori, J., and Somogyi, J. (1983). Differentiation of cerebellar mossy fiber synapses in the rat: a quantitative electron microscope study. J. Comp. Neurol. *220*, 365–377.

Harsch, A., and Robinson, H.P. (2000). Postsynaptic variability of firing in rat cortical neurons: the roles of input synchronization and synaptic NMDA receptor conductance. J. Neurosci. *20*, 6181–6192.

Hartzell, H.C., Kuffler, S.W., and Yoshikami, D. (1975). Post-synaptic potentiation: interaction between quanta of acetylcholine at the skeletal neuromuscular synapse. J. Physiol. *251*, 427–463.

Hausser, M., and Roth, A. (1997). Dendritic and somatic glutamate receptor channels in rat cerebellar Purkinje cells. J. Physiol. (Lond.) *501*, 77–95.

Heuser, J.E., Reese, T.S., Dennis, M.J., Jan, Y., Jan, L., and Evans, L. (1979). Synaptic vesicle exocytosis captured by quick freezing and correlated with quantal transmitter release. J. Cell Biol. *81*, 275–300.

Holmes, W.R. (1995). Modeling the effect of glutamate diffusion and uptake on NMDA and non-NMDA receptor saturation. Biophys. J. *69*, 1734–1747.

Hrabetova, S., Hrabe, J., and Nicholson, C. (2003). Dead-space microdomains hinder extracellular diffusion in rat neocortex during ischemia. J. Neurosci. *23*, 8351–8359.

Jahr, C.E. (2003). Drooling and stuttering, or do synapses whisper? Trends Neurosci. *26*, 7–9.

Jakab, R.L. (1989). Three-dimensional reconstruction and synaptic architecture of cerebellar glomeruli in the rat. Acta Morphol. Hung. *37*, 11–20.

Jakab, R.L., and Hamori, J. (1988). Quantitative morphology and synaptology of cerebellar glomeruli in the rat. Anat. Embryol. (Berl.) *179*, 81–88.

Jonas, P., Major, G., and Sakmann, B. (1993). Quantal components of unitary EPSCs at the mossy fibre synapse on CA3 pyramidal cells of rat hippocampus. J. Physiol. *472*, 615–663.

Katz, B. (1969). The Release of Neural Transmitter Substances (Liverpool, UK: Liverpool University Press).

Klyachko, V.A., and Jackson, M.B. (2002). Capacitance steps and fusion pores of small and large-dense-core vesicles in nerve terminals. Nature *418*, 89–92.

Krampfl, K., Schlesinger, F., Zorner, A., Kappler, M., Dengler, R., and Bufler, J. (2002). Control of kinetic properties of GluR2 flop AMPA-type channels: impact of R/G nuclear editing. Eur. J. Neurosci. *15*, 51–62.

Land, B.R., Harris, W.V., Salpeter, E.E., and Salpeter, M.M. (1984). Diffusion and binding constants for acetylcholine derived from the falling phase of miniature endplate currents. Proc. Natl. Acad. Sci. USA *81*, 1594–1598.

Longsworth, L.G. (1953). Diffusion measurements at 25° of aqueous solutions of amino acids, peptides and sugars. J. Am. Chem. Soc. *75*, 5705–5709.

Matsui, K., and Jahr, C.E. (2003). Ectopic release of synaptic vesicles. Neuron *40*, 1173–1183.

Min, M.Y., Rusakov, D.A., and Kullmann, D.M. (1998). Activation of AMPA, kainate, and metabotropic receptors at hippocampal mossy fiber synapses: role of glutamate diffusion. Neuron *21*, 561–570.

Mitchell, S.J., and Silver, R.A. (2000). GABA spillover from single inhibitory axons suppresses low-frequency excitatory transmission at the cerebellar glomerulus. J. Neurosci. *20*, 8651–8658.

Mitchell, S.J., and Silver, R.A. (2003). Shunting inhibition modulates neuronal gain during synaptic excitation. Neuron *38*, 433–445.

Mosbacher, J., Schoepfer, R., Monyer, H., Burnashev, N., Seeburg, P.H., and Ruppersberg, J.P. (1994). A molecular determinant for submillisecond desensitization in glutamate receptors. Science *266*, 1059–1062.

Nicholson, C., and Sykova, E. (1998). Extracellular space structure revealed by diffusion analysis. Trends Neurosci. *21*, 207–215.

Nicholson, C., and Tao, L. (1993). Hindered diffusion of high molecular weight compounds in brain extracellular microenvironment measured with integrative optical imaging. Biophys. J. *65*, 2277–2290.

Otis, T.S., Wu, Y.C., and Trussell, L.O. (1996). Delayed clearance of transmitter and the role of glutamate transporters at synapses with multiple release sites. J. Neurosci. *16*, 1634–1644.

Palay, S.L., and Chan-Palay, V. (1974). Cerebellar Cortex: Cortex and Organization (Berlin: Springer-Verlag).

Parsegian, V.A., Rand, R.P., and Rau, D.C. (1995). Macromolecules and water: probing with osmotic stress. Methods Enzymol. *259*, 43–94.

Partin, K.M., Fleck, M.W., and Mayer, M.L. (1996). AMPA receptor flip/flop mutants affecting deactivation, desensitization, and modulation by cyclothiazide, aniracetam, and thiocyanate. J. Neurosci. *16*, 6634–6647.

Perrais, D., and Ropert, N. (2000). Altering the concentration of GABA in the synaptic cleft potentiates miniature IPSCs in rat occipital cortex. Eur. J. Neurosci. *12*, 400–404.

Raman, I.M., and Trussell, L.O. (1995). The mechanism of alpha-amino-3-hydroxy-5-methyl-4-isoxazolepropionate receptor desensitization after removal of glutamate. Biophys. J. *68*, 137–146.

Raman, I.M., Zhang, S., and Trussell, L.O. (1994). Pathway-specific variants of AMPA receptors and their contribution to neuronal signaling. J. Neurosci. *14*, 4998–5010.

Ravindranathan, A., Donevan, S.D., Sugden, S.G., Greig, A., Rao, M.S., and Parks, T.N. (2000). Contrasting molecular composition and channel properties of AMPA receptors on chick auditory and brainstem motor neurons. J. Physiol. *523*, 667–684.

Renger, J.J., Egles, C., and Liu, G. (2001). A developmental switch in neurotransmitter flux enhances synaptic efficacy by affecting AMPA receptor activation. Neuron *29*, 469–484.

Rice, M.E., Okada, Y.C., and Nicholson, C. (1993). Anisotropic and heterogeneous diffusion in the turtle cerebellum: implications for volume transmission. J. Neurophysiol. *70*, 2035–2044.

Riveros, N., Fiedler, J., Lagos, N., Munoz, C., and Orrego, F. (1986). Glutamate in rat brain cortex synaptic vesicles: influence of the vesicle isolation procedure. Brain Res. *386*, 405–408.

Robert, A., and Howe, J.R. (2003). How AMPA receptor desensitization depends on receptor occupancy. J. Neurosci. *23*, 847–858.

Robinson, R.A., and Stokes, R.H. (2002). Electrolyte Solutions (New York: Dover).

Rusakov, D.A. (2001). The role of perisynaptic glial sheaths in glutamate spillover and extracellular Ca(2+) depletion. Biophys. J. *81*, 1947–1959.

Rusakov, D.A., and Fine, A. (2003). Extracellular Ca^{2+} depletion contributes to fast activity-dependent modulation of synaptic transmission in the brain. Neuron *37*, 287–297.

Rusakov, D.A., and Kullmann, D.M. (1998a). Extrasynaptic glutamate diffusion in the hippocampus: ultrastructural constraints, uptake, and receptor activation. J. Neurosci. *18*, 3158–3170.

Rusakov, D.A., and Kullmann, D.M. (1998b). Geometric and viscous components of the tortuosity of the extracellular space in the brain. Proc. Natl. Acad. Sci. USA *95*, 8975–8980.

Schoppa, N.E., and Westbrook, G.L. (2001). Glomerulus-specific synchronization of mitral cells in the olfactory bulb. Neuron *31*, 639–651.

Silver, R.A. (2003). Estimation of nonuniform quantal parameters with multiple-probability fluctuation analysis: theory, application and limitations. J. Neurosci. Methods *130*, 127–141.

Silver, R.A., Traynelis, S.F., and Cull-Candy, S.G. (1992). Rapid-time-course miniature and evoked excitatory currents at cerebellar synapses in situ. Nature *355*, 163–166.

Silver, R.A., Colquhoun, D., Cull-Candy, S.G., and Edmonds, B. (1996a). Deactivation and desensitization of non-NMDA receptors in patches and the time course of EPSCs in rat cerebellar granule cells. J. Physiol. *493*, 167–173.

Silver, R.A., Cull-Candy, S.G., and Takahashi, T. (1996b). Non-NMDA glutamate receptor occupancy and open probability at a rat cerebellar synapse with single and multiple release sites. J. Physiol. (Lond.) *494*, 231–250.

Stiles, J.R., Van Helden, D., Bartol, T.M., Jr., Salpeter, E.E., and Salpeter, M.M. (1996). Miniature endplate current rise times less than 100 microseconds from improved dual recordings can be modeled with passive acetylcholine diffusion from a synaptic vesicle. Proc. Natl. Acad. Sci. USA *93*, 5747–5752.

Syková, E. (2001). Glial diffusion barriers during aging and pathological states. Prog. Brain Res. *132*, 339–363.

Torri-Tarelli, F., Grohovaz, F., Fesce, R., and Ceccarelli, B. (1985). Temporal coincidence between synaptic vesicle fusion and quantal secretion of acetylecholine. J. Cell Biol. *101*, 1386–1399.

Wadiche, J.I., and Jahr, C.E. (2001). Multivesicular release at climbing fiber-Purkinje cell synapses. Neuron *32*, 301–313.

Watanabe, T., Ohtsuka, A., Murase, N., Barth, P., and Gersonde, K. (1996). NMR studies on water and polymer diffusion in dextran gels. Influence of potassium ions on microstructure formation and gelation mechanism. Magn. Reson. Med. *35*, 697–705.

Xu-Friedman, M.A., and Regehr, W.G. (2003). Ultrastructural contributions to desensitization at cerebellar mossy fiber to granule cell synapses. J. Neurosci. *23*, 2182–2192.

Zenisek, D., Steyer, J.A., Feldman, M.E., and Almers, W. (2002). A membrane marker leaves synaptic vesicles in milliseconds after exocytosis in retinal bipolar cells. Neuron *35*, 1085–1097.